Sharp Sides to the African Superplume

Sidao Ni*, Eh Tan, Michael Gurnis, Don Helmberger

Beneath southern Africa is a large structure about 1200 kilometers across and extending obliquely 1500 kilometers upward from the core-mantle boundary with a shear velocity reduction of about 3%. Using a fortuitous set of *SKS* phases that travel along its eastern side, we show that the boundary of the anomaly appears to be sharp, with a width less than 50 kilometers, and is tilted outward from its center. Dynamic models that fit the seismic constraints have a dense chemical layer within an upwardly flowing thermal structure. The tilt suggests that the layer is dynamically unstable on geological time scales.

The largest low-velocity structures in the lower mantle occur beneath southern Africa and the mid-Pacific. These low–shear wave velocity structures are correlated with hot spots (*1*), suggesting that the decrease in velocity is associated with an increase in temperature. The positive geoid anomaly and high topography over Africa (*2*, *3*) and the broad-scale Cenozoic uplift (*4*) are consistent with warm, rising mantle beneath Africa. However, recent tomographic imaging of the whole mantle suggests that bulk sound velocity and shear velocity (V_s) are negatively correlated within the African and Pacific anomalies (*5*), suggesting that the anomalies are chemical in origin, not thermal. The chemical hypothesis is supported by an inversion of normal modes (*6*) which indicates that the density of the lower mantle may increase within the two low V_s anomalies. If, over large scales (scale lengths of 1000 km), high-density chemical anomalies are embedded within thermal upwellings, as found in dynamic models (*7*–*9*), then we predict that there should be sharp jumps in seismic velocity, either radially or laterally, within the broad-scale low V_s structures delineated by seismic tomography. Here, we test this prediction with body wave seismology.

We search for rapid variations in V_s along paths between Africa and South America because of an ideal combination of earthquakes and seismic arrays that sample the African anomaly (*10*). Lowermost mantle structure can be distinguished from event mislocation and upper mantle structure using differential travel times of the phases S_cS and *SKS* relative to *S* (Fig. 1A). Anomalous patterns in $S_cS - S$ differential times, with delays as high as 10 s at epicentral distances beyond 90° (*11*, *12*), are not explained by tomographic models, which require sharpening and enhancing to produce such strong effects (Fig. 1B). Moreover, the travel times for the phase *SKS* can change rapidly when crossing the western and eastern boundaries of the African anomaly, with changes as large as several seconds between neighboring stations that have spacings of less than 50 km (Fig. 1C). When *SKS* data are modeled alone there is a trade off between thickness and velocity reduction that can be removed by adding the combination of $S_cS - S$ and $SKS - S$ data (*10*). Our preferred model fitting differential times and waveforms along this corridor is the LVZ2 model (Fig. 1A). It is a two-dimensional (2D) idealization of a large complex anomaly, which we will refer to as the African Low Velocity Structure (ALVS). The ALVS is aligned NW–SE and is about 1200 km wide, whereas the cross section LVZ2 extends at least 1200 km above the core-mantle boundary and leans toward the east between latitudes 15° and 30°S.

These large-scale features are apparent in seismic record sections. The sharpness of the western boundary (WB) is particularly evident from a rapid jump in travel times occurring near 100° for events recorded by the South African Array (Fig. 2A). Because the travel time jump occurs at different stations for other events, this feature is not related to shallow structure (*10*). A complementary travel time anomaly occurs for phases crossing the eastern boundary (EB), except that the

Seismological Laboratory, California Institute of Technology, Pasadena, CA 91125, USA.

*To whom correspondence should be addressed. E-mail: stone@gps.caltech.edu

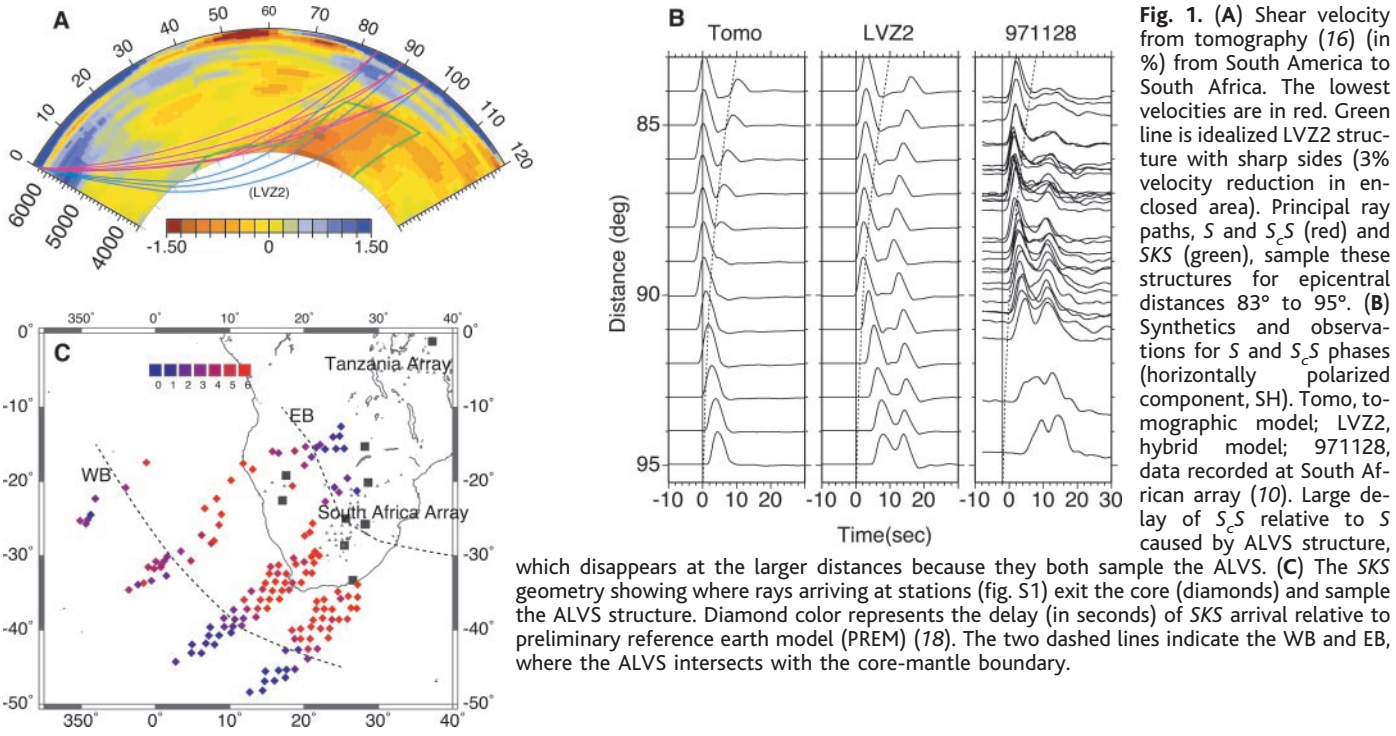

Fig. 1. (**A**) Shear velocity from tomography (*16*) (in %) from South America to South Africa. The lowest velocities are in red. Green line is idealized LVZ2 structure with sharp sides (3% velocity reduction in enclosed area). Principal ray paths, *S* and S_cS (red) and *SKS* (green), sample these structures for epicentral distances 83° to 95°. (**B**) Synthetics and observations for *S* and S_cS phases (horizontally polarized component, SH). Tomo, tomographic model; LVZ2, hybrid model; 971128, data recorded at South African array (*10*). Large delay of S_cS relative to *S* caused by ALVS structure, which disappears at the larger distances because they both sample the ALVS. (**C**) The *SKS* geometry showing where rays arriving at stations (fig. S1) exit the core (diamonds) and sample the ALVS structure. Diamond color represents the delay (in seconds) of *SKS* arrival relative to preliminary reference earth model (PREM) (*18*). The two dashed lines indicate the WB and EB, where the ALVS intersects with the core-mantle boundary.

jump in timing occurs in reverse order (Fig. 2B). *SKS* is delayed about 5 s for epicentral distances smaller than 97°; it becomes normal beyond 99°, as recorded by the Tanzanian Array, and is unlikely to be related to shallow structure (*10*).

The steepness of the *SKS* paths and their relative sharpness in delay times when crossing the edges of the ALVS are used to map out the boundaries. Although the arrival of *SKS* for large distances (>99°) is normal, it is late for small epicentral distances (<98°). Between 97° and 100°, the waveforms are broader (Fig. 2B). This pattern of waveform complication is probably caused by multipathing. For the shear velocity profile (Fig. 1A), the raypath of *SKS* around 97° is in the middle of the ALVS and yields a late *SKS* phase. However, for large epicentral distances (>100°), the raypath of *SKS* is outside ALVS and leads to normal arrivals. But when the raypath of *SKS* is close to the boundary of ALVS, two arrivals are produced: one from the ALVS and one from the surrounding higher velocity. If the boundary is sharp enough and the edge is nearly parallel to the raypath of *SKS*, a complicated waveform results. We demonstrate this phenomenon with 2D synthetic seismograms generated from the LVZ2 model (Fig. 2, C to E). For a sharp boundary with the edge almost parallel to a *SKS* raypath, complicated waveforms appear around 97° (Fig. 2C). But if the boundary is gradual (60 km or more), *SKS* waveforms lose their complexity (Fig. 2D). By comparing these synthetics with observed record sections, we estimate that the transition width should be less than 50 km. However, the slope of the edges is also important in controlling the shape of the waveforms. We explored the trade off between width and slope and found that *SKS* waveform distortion does not occur when the edge is not well aligned with the *SKS* raypath (Fig. 2E). Though the idealized synthetics display the waveform complexity over a short epicentral interval (about 1°), the observations indicate a broad zone. Part of this is caused by geometry; stations at the same epicentral distance are separated substantially in azimuth and, apparently, sample the wall differently.

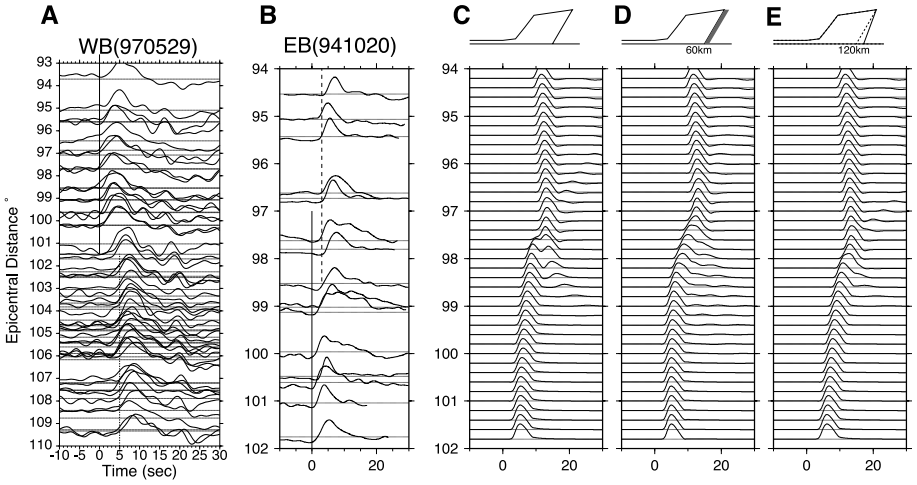

Fig. 2. (**A**) Record section sampling the WB edge for event 970529 with South African array. Solid lines, arrival times predicted by PREM; dotted lines are aligned with the delayed observations sampling the ALVZ. (**B**) Record section sampling the EB with the Tanzanian array. The travel time jumps are about 5 s and occur abruptly where the waveform data show evidence for multipathing (more than one arrival). (**C** to **E**) This possibility is explored synthetically by allowing a smooth transition from slow to normal at the EB edge. A sample of EB waveform data (B) showing the apparent multipathing is compared with synthetics on the right for various test cases. When the transition is thicker than about 60 km, the SKS synthetics change gradually with a few fat pulses near 98°. To produce some of the most disturbed observed waveforms requires a relatively sharp transition and a fortuitous geometry.

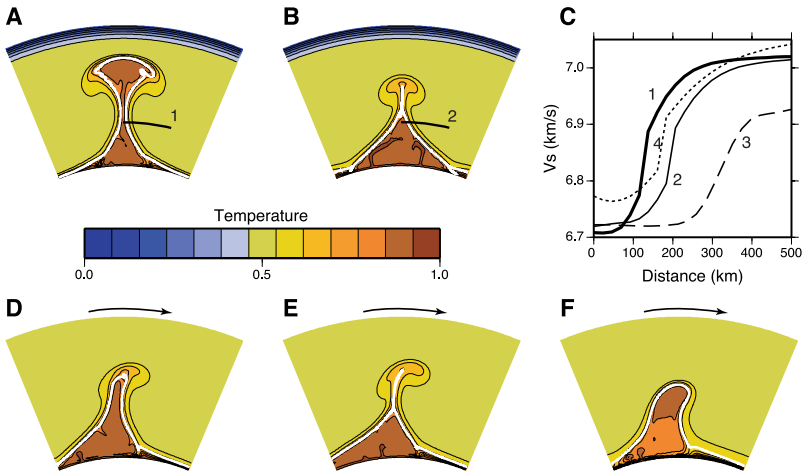

Fig. 3. Models of thermo-chemical convection (only central part of model domain shown). (**A**) $Ra = 10^7$, $B = 0.21$; (**B**) $Ra = 10^7$, $B = 0.23$. The white lines mark interface of chemical layer, which becomes stable for $B > 0.22$. (**C**) Modeled V_s at 2000 km depth. Profiles 1 [model in (A)] and 2 [in (B)] reproduce the sharp V_s reduction as observed. Profile 3 (fig. S4B) has insufficient V_s reduction, whereas profile 4 (fig. S4C) has sufficient V_s reduction but fails to reproduce *SKS* sharpness. (**D** to **F**) Models with an imposed plate velocity of ~1.5 cm/year (scaled to Earth). (D) $Ra = 10^7$, B = 0.21, the plume is sheared, but the right boundary is only slightly tilted outward; (E) $Ra = 10^7$, B = 0.23, a more stable chemical layer tilts less to the right. (F) $Ra = 10^7$, $B = 0.32$ with constant α. Only a very buoyant layer is capable of reproducing sharpness, tilt, and length scale of LVZ2.

We have attempted to simultaneously fit the observed sharpness and shape of the LVZ2 with models of mantle convection incorporating a plausible range of parameters. The models have a dense basal layer interacting with thermal convection, and they are controlled by the Rayleigh number (*Ra*) and the buoyancy number (*B*) (*10*). The influence of increasing *B* is to stabilize the dense layer while reducing the topography of the layer (*9*, *13*).

The chemical origin of the dense layer may be due to substitution of Mg by Fe in the mineral assemblage. Using relations between V_s and temperature and density, we transform model output into V_s (*10*, *14*). With no variations in chemistry and at relatively high *Ra* (10^7), seismic velocity variations occur over

a length scale of 200 km with a reduction in V_s of only 2% (Fig. 3C, profile 3). By assigning different seismic velocities across the chemical interface, we find a V_s decrease of almost 3% in a distance of 100 km, with half of the decrease occurring as an abrupt jump (Fig. 3C, profiles 1 and 2). For low Rayleigh number cases (10^6), similar structures are found but the chemical layer is embedded in a broad thermal halo (Fig. 3C, profile 4). We have not been able to find a purely thermal plume that produces an interface sharp enough to give the *SKS* multipathing; we conclude that it is more likely that the interface has a chemical origin.

The inclination of the interface is also diagnostic of the dynamics. If the dense basal layer is stable, then the interface between the two layers is always tilted toward the center of the anomaly (Fig. 3B). We find that the interface becomes tilted away from the central anomaly only when the chemical layer is unstable, that is, when the thermal buoyancy is greater than the chemical. Moreover, the two sides of the rising diapir are generally not parallel (as the seismic observations of Africa suggest); both sides become tilted inward near the base of the mantle and outward near the top of the diapir (Fig. 3A).

Alternatively, the inclination could be caused by a large-scale mode of convection, including flow associated with plate motion. Over the past 100 million years (My), Africa has moved northeastward in a hot spot frame of reference (*15*). This motion is in the same overall direction as the tilting of the ALVS (*16*). Although previous models have been able to reproduce the tilt of the ALVS, a tilt that may be caused by the shear associated with the African plate (*17*), they typically display diffuse mantle structures inconsistent with the sharpness implied by *SKS* multipathing. This result motivates a second class of dynamic models with an imposed velocity boundary condition simulating the northeastward motion of Africa (Fig. 3, D through F). The thermochemical anomaly with sharp edges can be tilted, but we have been unable to find plumes with subparallel sides (Fig. 3E) or with widths comparable to their heights (Fig. 3D). When the coefficient of thermal expansion (α) decreases with depth, we are unable to match the shape of LVZ2. When α decreases with depth, thermo-chemical plumes are unstable in the mid-mantle but stable in the lowermost mantle, and the plumes give rise to tilts distinctly different from those observed. However, with a uniform α, we are able to reproduce the shape of the LVZ2 (Fig. 3F). The structure has sharp boundaries tilted over in the direction of plate motion, subparallel sides, and a width comparable to its height. The better fit of cases with apparently unrealistic α suggests that a physical process is absent from the dynamic models. However, models with sharp boundaries and outwardly tilting edges are always transient because the dense chemical layer is being actively entrained upward. The implications of this result are important for the thermal and chemical evolution of the mantle.

References and Notes

1. M. A. Richards, B. H. Hager, N. H. Sleep, *J. Geophys. Res.* **93**, 7690 (1988).
2. B. H. Hager, R. W. Clayton, M. A. Richards, R. P. Comer, A. M. Dziewonski, *Nature* **313**, 541 (1985).
3. C. Lithgow-Bertelloni, P. G. Silver, *Nature* **395**, 269 (1998).
4. M. Gurnis, J. M. Mitrovica, J. Ritsema, H.-J. van Heijst, *Geochem. Geophys. Geosys.* **1**, 1 (2000).
5. G. Masters, G. Laske, H. Bolton, A. Dziewonski, in *Earth's Deep Interior*, S. I. Karato, Ed. (American Geophysical Union, Washington, DC, 2000), pp. 63–87.
6. M. Ishii, J. Tromp, *Science* **285**, 1231 (1999).
7. M. Gurnis, *J. Geophys. Res.* **91**, 11407 (1986).
8. U. Hansen, D. A. Yuen, *Nature* **334**, 237 (1988).
9. P. J. Tackley, in *The Core-Mantle Boundary Region*, M. Gurnis, M. E. Wysession, E. Knittle, B. A. Buffett, Eds. (American Geophysical Union, Washington, DC, 1998), pp. 231–253.
10. See supporting online material on *Science* Online at www.sciencemag.org/cgi/content/full/296/5574/1850/DC1.
11. S. Ni, D. Helmberger, *Earth Planet. Sci.* **187**, 301 (2001).
12. _____, *J. Geophys. Res.*, in press.
13. G. F. Davies, M. Gurnis, *Geophys. Res. Lett.* **13**, 1517 (1986).
14. I. Sidorin, M. Gurnis, in *The Core-Mantle Boundary Region*, M. Gurnis, M. E. Wysession, E. Knittle, B. A. Buffett, Eds. (American Geophysical Union, Washington, DC, 1998), pp. 209–230.
15. R. D. Müller, J.-Y. Royer, L. A. Lawver, *Geology* **21**, 275 (1993).
16. J. Ritsema, H. J. van Heijst, J. H. Woodhouse, *Science* **286**, 1925 (1999).
17. C. P. Conrad, M. Gurnis, *Geochem. Geophys. Geosys.*, in preparation.
18. A. M. Dziewonski, D. L. Anderson, *Phys. Earth Planet. Inter.* **25**, 297 (1981).

19. Supported by NSF grants EAR-00001966 and EAR-9725808.

8 February 2002; accepted 5 April 2002

Polytype Distribution in Circumstellar Silicon Carbide

T. L. Daulton,[1,2*†] T. J. Bernatowicz,[3] R. S. Lewis,[4] S. Messenger,[3] F. J. Stadermann,[3] S. Amari[3]

The inferred crystallographic class of circumstellar silicon carbide based on astronomical infrared spectra is controversial. We have directly determined the polytype distribution of circumstellar SiC from transmission electron microscopy of presolar silicon carbide from the Murchison carbonaceous meteorite. Only two polytypes (of a possible several hundred) were observed: cubic 3C and hexagonal 2H silicon carbide and their intergrowths. We conclude that this structural simplicity is a direct consequence of the low pressures in circumstellar outflows and the corresponding low silicon carbide condensation temperatures.

Presolar grains (*1*) are identified by the presence of elements with anomalous isotopic compositions that are distinct from the average solar mixture in a manner that cannot be produced by in situ nuclear processes such as radioactive decay, mass fractionation, or cosmic ray–induced spallation reactions. The inference is that these grains are produced in stellar ejecta, and their isotopic compositions, in part, reflect nucleosynthetic processes that occurred in their stellar sources.

The two most abundant forms of presolar grains isolated from primitive meteorites are nanometer-sized diamond (*2*) and micrometer- to submicrometer-sized SiC (*3*). Both are ubiquitous in primitive chondritic meteorites at 300 to 1800 parts per million (ppm) (diamond) and 1 to 28 ppm (SiC) (*4*). Silicon carbide is particularly interesting because it is known to form hundreds of different polytype structures in the laboratory, and the formation of a particular polytype is sensitive to growth conditions. Astronomical evidence of SiC in dusty envelopes of carbon stars comes from a relatively broad 11.3-μm infrared (IR) feature (*5*). However, attempts to distinguish from such IR spectra (*6–9*) whether α-SiC or β-SiC (*10*) predominates in carbon stars remain controversial (*11–15*).

Isotopic analysis of Si, C, N, and other elements in individual presolar SiC grains by ion microprobe shows that 99% of the SiC originated from low-mass asymptotic giant branch (AGB) stars of variable metallicity (with a small fraction possibly from J stars), whereas the other 1% came from supernovae (*1*, *16*). Here, we assume that presolar SiC grains from primitive meteorites can be taken to be a representative sample of the grain contributions from all kinds of stellar

[1]Materials Science Division, Argonne National Laboratory, Argonne IL, 60439–4838, USA. [2]Marine Geosciences Division, Naval Research Laboratory, Stennis Space Center, MS 39529–5004, USA. [3]Laboratory for Space Sciences, Washington University, St. Louis, MO 63130–4899, USA. [4]Enrico Fermi Institute, University of Chicago, Chicago, IL 60637–1433, USA.

*Present address: Naval Research Laboratory.
†To whom correspondence should be addressed. E-mail: tdaulton@nrlssc.navy.mil